PNAS
www.pnas.org

Main Manuscript for

A New Halogen Budget of the Bulk Silicate Earth Points to a History of Early Halogen Degassing Followed by Net Regassing

Meng Guo[1], Jun Korenaga[1]

[1]Department of Earth and Planetary Sciences, Yale University, New Haven, CT, USA.

Corresponding author: Meng Guo

Email: meng.guo@yale.edu

Author Contributions: M. G. performed the modeling and wrote the manuscript. J. K. designed the project, discussed the results, and commented on the manuscript.

Competing Interest Statement: The authors declare that they have no known competing financial interests or personal relationships that could have appeared to influence the work reported in this paper.

Classification: Physical sciences, planetary sciences

Keywords: Mantle composition, halogen cycle, early Earth

This PDF file includes:

Main Text
Figures 1 to 3
Tables 1

Abstract

Halogens are important tracers of various planetary formation and evolution processes, and an accurate understanding of their abundances in the Earth's silicate reservoirs can help us reconstruct the history of interactions among mantle, atmosphere, and oceans. The previous studies of halogen abundances in the bulk silicate Earth (BSE) are based on the assumption of constant ratios of element abundances, which is shown to result in a gross underestimation of the BSE halogen budget. Here we present a new, more robust approach using a log-log linear model. Using the new method, we provide an internally consistent estimate of halogen abundances in the depleted MORB-source mantle, the enriched OIB-source mantle, the depleted mantle, and BSE. Unlike previous studies, our results suggest that halogens in BSE are not more depleted compared to elements with similar volatility, thereby indicating sufficient halogen retention during planetary accretion. According to halogen abundances in the depleted mantle and BSE, we estimate that approximately ~87% of all stable halogens reside in the present-day mantle. Given our understanding of the history of mantle degassing and the evolution of crustal recycling, the revised halogen budget suggests that deep halogen cycle is characterized by efficient degassing in the early Earth and subsequent net regassing in the rest of Earth history. Such an evolution of deep halogen cycle presents a major step towards a more comprehensive understanding of ancient ocean alkalinity, which affects carbon partitioning within the hydrosphere, the stability of crustal and authigenic minerals, and the development of early life.

Significance Statement

Halogens play a critical role in biochemistry and are useful to understand how planets formed and evolved. As we found that the traditional way of constraining the halogen budget within Earth is unreliable, we developed a new method that better utilizes relevant geochemical data and estimated halogen abundances in various silicate reservoirs of Earth. Our new halogen budget indicates that the majority of halogens are more concentrated in the mantle than in the surface and suggests that halogens have likely experienced early degassing and subsequent net regassing. This study also provides an important key to deciphering the geological history of ocean chemistry.

Main Text

Introduction

The stable halogen elements (F, Cl, Br, and I) play a key role in a number of geochemical and biogeochemical systems. They affect the composition of hydrothermal fluids (e.g., *1*), the formation and transportation of ore minerals (e.g., *2, 3*), the composition of magmas (e.g., *4*), and the pathways of biochemical reaction (e.g., *5, 6*). Owing to their high volatility and incompatibility, halogens are also important tracers of planetary accretionary processes (e.g., *7*). A good understanding of halogen abundances in the bulk silicate Earth (BSE) and their current distribution among terrestrial reservoirs can help us track the history of interactions among mantle, crust, and hydrosphere (e.g., *8, 9*, *10*).

Previous studies of halogen abundances in BSE (e.g., *9, 11*, *12*, *13*) suggest that heavy halogens (Cl, Br, and I) display a noteworthy depletion compared to CI chondrites (*14*), by a factor of 30-50, which is far greater than expected from their condensation temperatures. Many attempts have been made to explain this severe depletion, including the models that require specific halogen behaviors during planetary accretionary processes (e.g., *13, 15, 16, 17*) and the reevaluation of halogen abundances in chondritic meteorites (*7*). Also, with the current BSE composition models, approximately 80% to 90% of Earth's halogens are concentrated in surface reservoirs (crust, oceans, and sediments) at present (e.g., *9, 18*). This unusually high degassing fraction is suggested to conflict with the mantle degassing fraction of ~50% based on argon-40 (*19*). Given that halogens are much more chemically active than argon, they can easily be incorporated into sediments, altered oceanic crust, and serpentinized mantle lithosphere and further be subducted into the mantle. Thus, their considerably high degassing fraction suggests unusual halogen behavior during Earth history (e.g., *7*). However, all of these efforts are built on the current estimates of BSE halogen budget. Therefore, there is an obvious impetus to examine the robustness of such estimates.

A common approach to estimate the halogen abundance in BSE employs the so-called constant ratio method (e.g., *9, 11, 12*). This method assumes that the ratios of halogen and some reference elements in mid-ocean-ridge basalts (MORB) and ocean island basalts (OIB) equal those in their respective source mantle. Thus, knowing the reference element concentration in the source mantle, the halogen concentrations can be calculated accordingly.

This method relies on the reference elements that are expected to behave similarly to halogens during melting and crystallization (e.g., K, Rb, and Pr). Strictly speaking, however, the constant ratio method can adequately be applied only in one specific situation: when the bulk distribution coefficients of halogens and reference elements are the same during both mantle melting and magma crystallization. Only in this case, halogen and the reference element are linearly related, or in other words, the logarithmic slope of their covariation becomes unity. Unfortunately, such delicate equivalence is not observed in the MORB nor the OIB dataset (Tables S1 and S2).

The limitation of the constant ratio method can be illustrated by modeling how halogen concentrations in MORB or OIB may be related to those in the respective source mantle through mantle melting (Fig. 1A) and crystallization (Fig. 1B). The calculated abundances of halogens and reference elements in the source mantle depend on their bulk distribution coefficients, and different assumptions on these distribution coefficients result in different slopes of covariations in the log-log space (Figs. 1A and 1B). As noted before, the logarithmic slope of halogen and reference element is unity only when their bulk distribution coefficients are the same, and the slope deviates more from unity with increasingly dissimilar bulk distribution coefficients. As can be seen from the MORB and OIB datasets (Tables S1 and S2), most of pairs of halogens and reference elements used in previous studies (e.g., F vs. Pr, F vs. K, Cl vs. K, and Cl vs. Rb) display nonlinear covariations, with their logarithmic slopes smaller than unity, which indicate considerably higher halogen concentrations in the source mantle compared with what the constant ratio method provides. In other words, the constant ratio method underestimates halogen abundances in the primary melt (Fig. 1A) and the source mantle (Fig. 1B) of MORB and OIB.

In light of the above, we have developed a new method to better constrain halogen abundance in Earth's silicate reservoirs. This new method applies the log-log linear model of halogen and reference elements in MORB and OIB to estimate the halogen abundances in the respective source mantle (e.g., blue lines in Figs. 1B and 1C). In this study, we consider the following four kinds of source mantle. The bulk silicate Earth (BSE) refers to the chemical composition of mantle after core segregation and before the extraction of continental crust (CC); BSE is synonymous with the primitive mantle (PM). The depleted mantle (DM) denotes the

residual mantle after the extraction of CC from BSE and can be further divided into the depleted MORB-source mantle (DMM) and the enriched OIB-source mantle (EM). DMM is more depleted in trace elements compared to EM.

By exploiting nonlinear correlations exhibited by MORB and OIB, our new method can bypass the uncertainties of the bulk distribution coefficients of halogens during both mantle melting and melt crystallization (e.g., *20*), and, compared to the constant ratio method, our approach results in notably higher halogen abundance in DMM and EM according to the MORB and OIB datasets (*21*). In contrast to previous studies, this higher estimate suggests that halogen is not notably depleted in BSE compared to CI chondrites given their condensation temperatures, which indicates effective halogen preservation during planetary formation. Considering the history of mantle degassing (e.g., *22*) and the evolution of crustal recycling (e.g., *23*), our new estimate also suggests a halogen cycle of early degassing followed by a net regassing during the Earth history, which provides important implications for the evolution of ocean alkalinity and pH.

In what follows, we first present a brief description of the new method based on a log-log linear model, then summarize the model results, and discuss the implications of our new estimate of halogen abundance in BSE. The full description of the new method and a detailed discussion on the problems of the constant ratio method are given in Methods.

Results

In addition to the use of a log-log linear model, our new method is designed to obtain internally-consistent halogen abundances in DMM, EM, DM, and BSE. For each halogen element, we first choose several reference elements, which have sufficiently high correlation coefficients with halogens in the log-log space (Tables S1 and S2) and have good constraints on their abundances in CC, DMM, and BSE. A subset of the covariations between halogens and reference elements in MORB and OIB and their corresponding log-log linear models are shown in Fig. 2, whereas the complete set of our results is provided in Figs. S1 to S5.

To make an internally consistent estimate of halogen abundances in Earth's silicate reservoirs, we then take the following five steps. First, according to the abundances of reference elements in CC (*24*) and BSE (*12*), we calculate their concentrations in DM using mass balance.

Second, we calculate their concentrations in EM given their compositions in DM and DMM (*25*). Third, we obtain the halogen concentrations in DMM and EM using their log-log linear models with reference elements in MORB and OIB, respectively. Subsequently, the halogen compositions in DM can be calculated by summing their abundances in DMM and EM. Finally, we provide an estimate of BSE halogen budget by adding their abundances in surface reservoirs (*9, 24, 26-29*). Throughout these five steps, we use Monte Carlo sampling to incorporate the uncertainties of the relative proportion of DMM and EM (e.g., *30, 31*), correlations between halogens and reference elements in MORB and OIB, and element concentrations in DMM (*25*), CC (*24*), and BSE (*12*). We have collected a total of 10,000 Monte Carlo sampling results, whose median and standard deviation are reported in Table 1.

For the DMM composition, the models of Salters and Stracke (*25*) and Workman and Hart (*32*) have widely been used in the literature. In our analysis, we chose to use the former, because the latter was found to result in negative EM abundances for some reference elements (e.g., Rb). The results in Table 1 are based on the assumption that DMM is the source mantle of MORB, whereas EM is the source mantle of OIB. We also tested the assumption that OIB was generated directly from BSE (which is synonymous with PM), and the corresponding results are provided in Table S3, which displays higher halogen budgets in BSE. As seen in Tables 1 and S3, our new method results in ~2-9 times higher halogen concentrations in BSE compared to previous studies (e.g., *9*, *11*, *12*, *13*).

Given the halogen abundances in DM and BSE, we calculate their degassing fractions in the present-day mantle (Tables 1 and S3). Our new BSE estimate suggests that less than half of each halogen have been degassed from the primitive mantle, with iodine as an exception (~80%). A total amount of ~87% stable halogens still reside in the mantle. Studies on halogen concentrations in serpentinites suggest that iodine and bromine are lost from serpentinites at shallower depths than chlorine and fluorine (e.g., *33*), which may be responsible for the higher degassing fractions of heavier halogens (Tables 1 and S3). Also, the calculated degassing fraction of iodine suggests that OIB cannot be generated directly from the primitive mantle (Table S3). Whereas this high degassing fraction of iodine is subject to large uncertainties given the paucity of iodine data in the MORB and OIB datasets (Tables S1 and S2), a better understanding of the mineral-melt-fluid partitioning of iodine is also warranted.

Discussion

As mentioned in the Introduction, previous studies of BSE halogen concentrations (e.g., *9, 11, 12, 13*) exhibit a noteworthy depletion of Cl, Br, and I (green dots in Fig. 3), considering their condensation temperatures (*14*). This depletion has long been thought to require some peculiar halogen behaviors, including halogen sequestration into the core (*15, 16*), the lower condensation temperatures of halogens (*17*), and an impact-driven loss of halogens in the early Earth (*13*). However, our revised halogen abundances in BSE yield considerably higher CI-chondrite normalized values (red dots in Fig. 3), indicating that BSE is not unusually depleted in halogens. Thus, our results suggest sufficient halogen retention during planetesimal formation and giant impacts. Recently, Clay et al. (*7*) reexamined the abundances of chlorine, bromine, and iodine in various kinds of chondrites and reported much lower averaged concentrations of halogens. Normalizing our estimates to the chondrite values of Clay et al. (*7*) results in a halogen volatility trend slightly above the volatile lithophile elements with similar condensation temperatures (yellow dots in Fig. 3). The halogen concentrations of CI chondrites may not be as low as suggested by Clay et al. (*7*).

The previous estimates of the BSE budget yield a halogen degassing fraction of ~80% from the present-day mantle (e.g., *9, 18*), which is considered to conflict with the mantle degassing fraction of ~50% based on argon-40 (*19*). On the other hand, our results suggest much lower degassing fractions of halogens (~5% for F to ~47% for Br). It is important to understand that the degassing fractions of argon-40 and halogens do not have to be the same to begin with. First of all, unlike argon-40, halogens are not radiogenic; therefore, their degassing history can be more affected by early degassing events caused by giant impacts (e.g., *34*) and early intensive crustal generation and reworking (*22*). Argon-40, in contrast, did not exist in abundance in the early Earth because it is produced by the radioactive decay of potassium-40 with a half-life of over one billion years, so its present-day budget in the convecting mantle is much less sensitive to such early degassing. As fluorine and chlorine are most likely degassed in the form of HF and HCl, respectively, their degassing behavior is expected to be similar to that of water (*35*). Thus, based on water degassing expected during magma ocean solidification and subsequent mantle convection (e.g., *36, 37*), halogens are likely to have been degassed efficiently during the Hadean. Moreover, halogens are more chemically active than argon and can be recycled into the mantle by chemically bonding to minerals. Thus, the lower degassing fraction of halogens

suggested by our new BSE budget is consistent with net halogen regassing due to the recycling of both oceanic crust (e.g., *23*) and continental crust (e.g., *22*). A similar regassing history is reported for xenon (*38*) as well. The majority of halogens in the present-day mantle originally brought as subducted materials may exist along grain boundaries or in some trace minerals because nominally anhydrous minerals in mantle peridotites do not seem to contain a sufficient amount of halogens (*39*). As high concentrations of halogens are observed in both MORB and OIB, such mantle components enriched in halogens should be ubiquitous in the convecting mantle, though our study does not constrain their specifics.

To sum, our new estimates suggest that the exchange of halogens between the surface and the interior is described by early degassing followed by net regassing through the rest of Earth history. Deep volatile cycle on Earth has long been investigated, as it can provide a framework for studying the long-term geochemical evolution of mantle, crust, and hydrosphere (e.g., *8, 9, 10, 40*). Quantitative analyses have been conducted for quite a few elements, including water (e.g., *37, 40*), carbon (e.g., *41,42*), sulfur (e.g., *43*), nitrogen (e.g., *44*), and noble gases (e.g., *22, 38*). The proposed degassing history of halogens is a preliminary attempt in this thread of research, and future directions include the modeling of deep halogen cycle in conjunction with other geochemical and geophysical constraints and its application to relevant geological processes. For example, deciphering the evolution of ocean pH requires the understanding of both carbon and halogen cycles.

The geological history of ocean pH is critical in understanding the long-term habitability of Earth, because it controls carbon partitioning within hydrosphere (*45*), biosynthetic pathways (*46*), and the stability of crustal and authigenic minerals (*47*). However, the early Earth environment is highly debated, with temperature estimates ranging from icy to hot (e.g., *41, 48*) and ocean pH estimates fluctuating between strongly acidic to alkaline (*41, 49, 50*). To constrain the evolving seawater pH, one need to solve the charge balance of the major seawater ions (e.g., *51*), including Na^+, Mg^{2+}, Cl^-, CO_3^{2-}, and SO_4^{2-}. Therefore, as one of the most important acids in the ocean, an accurate understanding of the outgassing history of chlorine is required to constrain the chemical properties of seawater. Previous efforts on constraining acid-base balance of the oceans mainly focus on exploring the effect of atmospheric pCO_2 (e.g., *52*), whereas the exchanges of chlorine among Earth reservoirs are parameterized simply by assuming a certain model for the thermal evolution of Earth (*51*). Modeling the history of

239 halogen degassing based on our new estimate of BSE budget will be an important step towards
240 a comprehensive understanding of the geological history of ocean pH.

241 As explained in the Introduction, the constant ratio method is useful when estimating
242 concentrations for element pairs with the same bulk distribution coefficients, but this
243 requirement for bulk distribution coefficients is not easily satisfied. Because the constant ratio
244 method has widely been used when building the compositional models of the depleted MORB-
245 source mantle (*25*, *32*), the continental crust (e.g., *24*), and the bulk silicate Earth (e.g., *11, 12*), it
246 is important to revisit the validity of the constant ratio approach in those models. Our new
247 halogen budget, which depends on the models of major silicate reservoirs, must be seen as
248 provisional until these models are thoroughly reexamined. The impact of this model
249 dependence on our results is, however, likely to have been alleviated by incorporating various
250 model uncertainties with Monte Carlo sampling. As many geochemical box models depend
251 critically on global mass balance, an improved understanding of compositional models is
252 essential for reconstructing global-scale geological processes.

253

254 **Methods**
255
256 **1. Problems with the constant ratio method**

257 As mentioned in the Introduction, the ratio of halogen and reference element in MORB and
258 OIB is used to calculate the halogen concentration in the respective source mantle, but this can
259 lead to a severe underestimation. To demonstrate this point, we consider element
260 concentrations in DMM and EM by assuming a two-stage model: the source mantle first
261 generates primary melt, which then evolves to MORB or OIB through fractional crystallization.
262 We begin with back-calculating element abundances in the primary melt from the composition
263 of MORB or OIB. Here we take the observed abundances of fluorine (F) and potassium (K) in
264 MORB as an example, and their concentrations in the primary melt can be calculated as:

265 $$C_{\mathrm{l}}(\mathrm{F}) = \frac{C_{\mathrm{MORB}}(\mathrm{F})}{f_{\mathrm{C}}^{(D_{\mathrm{C}}(\mathrm{F})-1)}}; \quad (1)$$

266 $$C_{\mathrm{l}}(\mathrm{K}) = \frac{C_{\mathrm{MORB}}(\mathrm{K})}{f_{\mathrm{C}}^{(D_{\mathrm{C}}(\mathrm{K})-1)}}, \quad (2)$$

where C_{l} is the element concentration in the primary melt before fractional crystallization, C_{MORB} is the element concentration observed in MORB (black dot in Fig. 1A), f_{C} and D_{C} are the melting fraction and bulk distribution coefficient during the fractional crystallization of primary melt. By taking the logarithm of equations (1) and (2) and eliminating $\ln(f_{\mathrm{C}})$, the logarithmic concentrations of F and K in the primary melt are related as:

$$\ln(C_{\mathrm{l}}(\mathrm{F})) = s\ln(C_{\mathrm{l}}(\mathrm{K})) + \ln\left(\frac{C_{\mathrm{MORB}}(\mathrm{F})}{C_{\mathrm{MORB}}(\mathrm{K})^{s}}\right), \quad (3)$$

where the slope, s, is a function of the bulk distribution coefficients of F and K:

$$s = \frac{D_{\mathrm{C}}(\mathrm{F})-1}{D_{\mathrm{C}}(\mathrm{K})-1}. \quad (4)$$

By varying f_{C} and D_{C}, we calculate the possible concentrations of F and K in the primary melt. As can be seen from equation (4) and Fig. 1A, the slope of F and K in the primary melt is unity only when $D_{\mathrm{C}}(\mathrm{F})$ and $D_{\mathrm{C}}(\mathrm{K})$ are the same, which is what is assumed by the constant ratio method. In contrast, most of the observed log-covariations of halogen and reference elements in MORB and OIB exhibit a slope much less than unity (Tables S1 and S2), which is equivalent to considerably higher halogen abundances in the primary melt.

We next consider the relation between the source mantle composition and the primary melt composition. Continuing with elements F and K, their concentrations in the source mantle may be calculated as:

$$C_{\mathrm{SM}}(\mathrm{F}) = \frac{C_{\mathrm{l}}(\mathrm{F})f_{\mathrm{M}}}{1-(1-f_{\mathrm{M}})^{\frac{1}{D_{\mathrm{M}}(\mathrm{F})}}}; \quad (5)$$

$$C_{\mathrm{SM}}(\mathrm{K}) = \frac{C_{\mathrm{l}}(\mathrm{K})f_{\mathrm{M}}}{1-(1-f_{\mathrm{M}})^{\frac{1}{D_{\mathrm{M}}(\mathrm{K})}}}, \quad (6)$$

where C_{SM} is the element concentration in the source mantle of MORB, C_{l} is the element concentration in the primary melt (black dots in Fig. 1B), and f_{M} and D_{M} are melt fraction and bulk distribution coefficient during fractional melting (*53*). By varying f_{M} and D_{M}, the concentrations of F and K in the MORB source mantle display a range of log-correlations (Fig. 1B), and we calculate the corresponding F concentrations in DMM (grey dots in Fig. 1B) using K abundance (grey bar in Fig. 1B).

The ratios of element concentrations in MORB and DMM equal to each other only when the bulk distribution coefficients of relevant elements are the same during both mantle melting and subsequent crystallization (Fig. 1B), which is required for the constant ratio method to be safely applied. However, the MORB and OIB data do not provide any pair of elements with a logarithmic slope of unity (Tables S1 and S2), undermining the validity of the constant ratio method. Also, the covariation of element concentrations can change during mantle melting and crystallization, when their bulk distribution coefficients are different (Figs. 1A and 1B). This suggests that even the observed log-linear relationship of element abundances in MORB or OIB may not simply be extrapolated to estimate halogen abundances in the respective source mantle. In summary, using the constant ratio method will cause severe underestimation of halogen abundances in DMM and EM.

2. A new method based on a log-log linear model

Our new method uses log-linear covariations between halogens and reference elements in MORB and OIB to estimate halogen abundances in their respective mantle. The bulk distribution coefficients of halogens can vary during both melting and crystallization (e.g., *20*), thus the simple extrapolation used in our new method (dashed blue line in Fig. 1B) may be simplistic, but most of correlations considered here extend down to the level of concentration expected for a source mantle (Fig. 2 and Figs. S1-S5). It is thus notable that, for any given pair of halogen and reference element with a logarithmic slope smaller than unity, the new method results in considerably higher halogen abundances compared to the constant ratio method (Fig. 1C). The slope of the observed log-log linear model depends on the bulk distribution coefficients of both halogen and reference element (equation (4)), whereas the y-intercept reflects the average concentration of halogen in MORB or OIB (equation (3)). As both MORB and OIB are generally more evolved than their primary melts, the observed log-log linear relationships are dictated by fractional crystallization.

Based on the relationship of logarithm slopes and the bulk distribution coefficients of relevant elements (equation (4)), the bulk distribution coefficients of halogens between mineral assemblage and basaltic melt can be estimated. As the reference elements used in our study are all highly incompatible, i.e., $D \ll 1$, the distribution coefficient for halogen may simply be estimated as 1-*s*, where *s* is the logarithmic slope. Estimated bulk distribution coefficients are

~0.55 for fluorine, ~0.5 for chlorine, ~0.35 for bromine, and ~0.3 for iodine. Heavier halogens are more incompatible, which is consistent with trends seen in experimental results. However, experimentally determined mineral-melt partition coefficients are lower often by more than one order of magnitude for nominally anhydrous minerals relevant to the solidification of basaltic melt (e.g., *54, 55*). We note that the published partitioning experiments were conducted at pressures higher than those relevant to crystallization within the oceanic crust, and that the pressure dependence of partitioning is indicated by some experimental data (*54*). Moreover, based on natural samples, Urann et al. (*39*) estimated the inter-mineral partitioning of fluorine and chlorine between mantle minerals, which differs significantly from what is suggested by the partitioning experiments. In our analysis, correlations involving chlorine are admittedly noisy likely because of seawater contamination as well as the assimilation of altered oceanic crust. However, correlations involving other halogens do not suffer from the same issue. Thus, the logarithmic correlations reported in this study may be considered as novel empirical constraints on the partitioning of these halogens, at least for the low-pressure fractionation of basaltic melt.

For each halogen element, we choose multiple reference elements to estimate the halogen abundance in BSE based on a log-log linear model. Reference elements are selected according to the following two criteria: (1) they have good correlation in the log-log space with halogen in both MORB and OIB (Table S1 and S2), and (2) they have well-constrained abundances in DMM, CC, and BSE. The concentrations of halogen and reference elements in MORB and OIB are taken from PetDB (*21*) using off-axis spreading center and spreading center as tectonic settings for MORB dataset, whereas aseismic ridge, oceanic plateau, ocean island, and seamount for OIB dataset. The data are further selected by their MgO contents, to be within the range of 5% to 15%.

Taking fluorine and potassium as an example again, we apply the following five steps, with log-log linear models and Monte Carlo sampling, to estimate F abundances in DMM, EM, DM, and BSE. First, by using the mass balance among DM, CC, and BSE, we calculate the concentration of K in DM as follows:

$$C_{\mathrm{DM}}(\mathrm{K})M_{\mathrm{DM}} = C_{\mathrm{BSE}}(\mathrm{K})M_{\mathrm{BSE}} - C_{\mathrm{CC}}(\mathrm{K})M_{\mathrm{CC}}, \quad (7)$$

where $C_{\mathrm{BSE}}(\mathrm{K})$ and $C_{\mathrm{CC}}(\mathrm{K})$ are the concentrations of K in BSE (*12*) and CC (*24*), respectively. Using Monte Carlo sampling, we take into account the uncertainties of element concentrations in BSE and CC. The masses of BSE (M_{BSE}) and CC (M_{CC}) are 4.0359 x 10^{24} kg and 2.09 x 10^{22} kg, respectively, whereas the mass of DM (M_{DM}) is the difference between M_{BSE} and M_{CC}.

Second, we calculate the concentration of K in EM ($C_{\mathrm{EM}}(\mathrm{K})$) using the mass balance among DMM, EM, and DM as follows:

$$C_{\mathrm{EM}}(\mathrm{K})M_{\mathrm{EM}} = C_{\mathrm{DM}}(\mathrm{K})M_{\mathrm{DM}} - C_{\mathrm{DMM}}(\mathrm{K})M_{\mathrm{DMM}}, \quad (8)$$

where the concentration of potassium in DMM (C_{DMM}) is taken from Salters and Stracke (*25*). We incorporate the uncertainties of C_{DMM} and the relative proportion of M_{DMM} and M_{EM} using Monte Carlo sampling, where M_{DMM} is considered to be within the range of 70% $\pm$ 20% of M_{DM} (e.g., *30, 31*).

Third, we calculate the concentrations of F in DMM and EM ($C_{\mathrm{DMM}}(\mathrm{F})$ and $C_{\mathrm{EM}}(\mathrm{F})$) based on a log-log linear model as follows:

$$C_{\mathrm{DMM}}(\mathrm{F}) = s_{\mathrm{MORB}}C_{\mathrm{DMM}}(\mathrm{K}) + b_{\mathrm{MORB}}, \quad (9)$$

$$C_{\mathrm{EM}}(\mathrm{F}) = s_{\mathrm{OIB}}C_{\mathrm{EM}}(\mathrm{K}) + b_{\mathrm{OIB}}, \quad (10)$$

where s and b are the log-slope and y-intercept of F and K covariation in MORB or OIB, respectively. The error envelopes of the log-log linear models are incorporated using Monte Carlo sampling. During this step, we use several reference elements for each halogen element to constrain their concentrations and take the medians as the halogen concentrations in DMM and EM.

Fourth, we estimate halogen abundance in the present-day DM ($C_{\mathrm{DM}}(\mathrm{F})$) as follows:

$$C_{\mathrm{DM}}(\mathrm{F})M_{\mathrm{DM}} = C_{\mathrm{DMM}}(\mathrm{F})M_{\mathrm{DMM}} + C_{\mathrm{EM}}(\mathrm{F})M_{\mathrm{EM}}, \quad (11)$$

where M_{DMM} and M_{EM} are those sampled in the second step.

Last, by adding the abundances of halogen in Earth's surface reservoirs, we calculated the total halogen concentrations in BSE:

$$C_{\mathrm{DM}}(\mathrm{F})M_{\mathrm{DM}} + C_{\mathrm{SW}}(\mathrm{F})M_{\mathrm{SW}} + C_{\mathrm{EV}}(\mathrm{F})M_{\mathrm{EV}} + C_{\mathrm{CB}}(\mathrm{F})M_{\mathrm{CB}} + C_{\mathrm{MS}}(\mathrm{F})M_{\mathrm{MS}} + C_{\mathrm{CC}}(\mathrm{F})M_{\mathrm{CC}} = C_{\mathrm{BSE}}(\mathrm{F})M_{\mathrm{BSE}}, \quad (12)$$

where C_{SW}, C_{EV}, C_{CB}, C_{MS}, and C_{CC} are the concentrations of halogen in seawater *(9)*, evaporites (*28*), crustal brines (*26, 27*), marine sediments (*29*) and continental crust (*24*), respectively, and M_{SW}, M_{EV}, M_{CB}, M_{MS}, M_{CC} denote the masses of these reservoirs (Table 1). By construction, these five steps provide us an internally consistent estimate of halogen abundances in EM, DMM, DM, and BSE.

Acknowledgments

This article is supported by National Science Foundation under grant EAR-1753916 and the U.S. National Aeronautics and Space Administration under Cooperative Agreement No. 80NSSC19M0069 issued through the Science Mission Directorate. We thank the editor and two anonymous reviewers for constructive comments.

References

1. M. A. Kendrick, "Halogens in seawater, marine sediments and the altered oceanic lithosphere" in The Role of Halogens in Terrestrial and Extraterrestrial Geochemical Processes: Surface, Crust, and Mantle, D. E. Harlov, L. Aranovich, Eds, Springer, Cham (2018), pp. 591-648.
2. D. R. Baker, H. Balcone-Boissard, Halogen diffusion in magmatic systems: Our current state of knowledge. *Chem. Geol.*, **263**, 82-88 (2009).
3. P. Lecumberri-Sanchez, R. J. Bodnar, "Halogen geochemistry of ore deposits: contributions towards understanding sources and processes" in The Role of Halogens in Terrestrial and Extraterrestrial Geochemical Processes: Surface, Crust, and Mantle, D. E. Harlov, L. Aranovich, Eds, Springer, Cham (2018), pp. 261-305.
4. D. Dolejš, Z. Zajacz, "Halogens in silicic magmas and their hydrothermal systems" in The Role of Halogens in Terrestrial and Extraterrestrial Geochemical Processes: Surface, Crust, and Mantle, D. E. Harlov, L. Aranovich, Eds, Springer, Cham (2018), pp. 431-543.
5. R. Fuge, "Soils and iodine deficiency" in Essentials of Medical Geology, O. Selinus, B. Alloway, J. A. Centeno, R. B. Finkelman, R. Fuge, U. Lindh, P. Smedley, Eds, Elsevier Academic Press, Amsterdam (2005), pp. 417-433.
6. G. M. El Zokm, M. M. Ismail, G. F. El-Said, Halogen content relative to the chemical and biochemical composition of fifteen marine macro and micro algae: nutritional value, energy supply, antioxidant potency, and health risk assessment. *Environ. Sci. Pollut. Res.*, **28**, 14893-14908 (2021).
7. P. L. Clay, R. Burgess, H. Busemann, L. Ruzié-Hamilton, B. Joachim, J. M. Day, C. J. Ballentine, Halogens in chondritic meteorites and terrestrial accretion. *Nature*, **551**, 614-618 (2017).
8. R. D. Jarrard, Subduction fluxes of water, carbon dioxide, chlorine, and potassium. *Geochem. Geophys. Geosystems*, ***4*** (2003).
9. M. A. Kendrick, C. Hémond, V. S. Kamenetsky, L. Danyushevsky, C. W. Devey, T. Rodemann, M. A. Jackson, M. R. Perfit, Seawater cycled throughout Earth's mantle in partially serpentinized lithosphere. *Nat. Geosci.*, **10**, 222-228 (2017).

10. H. Tang, D. Trail, E. A. Bell, T. M. Harrison, Zircon halogen geochemistry: Insights into Hadean-Archean fluids. *Geochem. Perspect. Lett.*, **9**, 49-53 (2019).
11. W. F. McDonough, S. S. Sun, The composition of the Earth. *Chem. Geol.*, **120**, 223-253 (1995).
12. T. Lyubetskaya, J. Korenaga, Chemical composition of Earth's primitive mantle and its variance: 1. Method and results. *J. Geophys. Res. Solid Earth*, **112**, B03211 (2007).
13. Z. D. Sharp, D. S. Draper, The chlorine abundance of Earth: implications for a habitable planet. *Earth Planet. Sci. Lett.,* **369**, 71-77 (2013).
14. K. Lodders, Solar system abundances and condensation temperatures of the elements. *Astrophys. J.*, **591**, 1220–1247 (2003).
15. W. F. McDonough, "Compositional model for the Earth's core" in Treatise on Geochemistry, R. W. Carlson, Eds, Elsevier-Pergamon, Oxford (2003), pp. 547–568.
16. R. M. G. Armytage, A. P. Jephcoat, M. A. Bouhifd, D. Porcelli, Metal-silicate partitioning of iodine at high pressures and temperatures: implications for the Earth's core and ^{129}Xe budgets. *Earth Planet. Sci. Lett.,* **373**, 140–149 (2013).
17. M. Y. Zolotov, M. Mironenko, Hydrogen chloride as a source of acid fluids in parent bodies of chondrites. *Lunar Planet. Sci. Conf.*, **38,** 2340 (2007).
18. R. Burgess, E. Layzelle, G. Turner, J. W. Harris, Constraints on the age and halogen composition of mantle fluids in Siberian coated diamonds. *Earth Planet. Sci. Lett.,* **197**, 193-203 (2002).
19. C. J. Allègre, A. Hofmann, and K. O'Nions, The argon constraints on mantle structure. *Geophys. Res. Lett.*, **23**, 3555-3557 (1996).
20. J. D. Webster, D. R. Baker, A. Aiuppa, "Halogens in mafic and intermediate-silica content magmas" in The Role of Halogens in Terrestrial and Extraterrestrial Geochemical Processes: Surface, Crust, and Mantle, D. Harlow, L.Y. Aranovich, Eds, Springer International Publishing (2018), pp. 307-430.
21. The data were downloaded from the PetDB Database (https://search.earthchem.org/) on 25th Jan, 2021.
22. M. Guo, J. Korenaga, Argon constraints on the early growth of felsic continental crust. *Sci. Adv.*, ***6***, eaaz6234 (2020).

44923. S. B. Shirey, R. W. Carlson, S. H. Richardson, A. Menzies, J. Gurney, D. G. Pearson, J.
450 W. Harris, U. Wiechert, Archean emplacement of eclogite components into the
451 lithospheric mantle during formation of the Kaapvaal Craton. *Geophys. Res. Lett*., **28**,
452 2509–2512 (2001).
45324. Rudnick, R. L., Gao, S., "Composition of the Continental Crust" in *Treatise on*
454 *Geochemistry* Vol. 3, H. D. Holland, K. K. Turekian, Eds, Pergamon (2003), pp. 1–64.
45525. V. J. Salters, A. Stracke, Composition of the depleted mantle. *Geochem. Geophys.*
456 *Geosystems*, **5** 2004.
45726. M. A. Kendrick, D. Phillips, M. Wallace, J. M. Miller, Halogens and noble gases in
458 sedimentary formation waters and Zn-Pb deposits: A case study from the Lennard Shelf,
459 Australia. *Appl. Geochem.*, **26**, 2089-2100 (2011).
46027. R. H. Worden, Controls on halogen concentrations in sedimentary formation waters.
461 *Mineral. Mag.*, **60**, 259-274 (1996).
46228. W. W. Hay, A. Migdisov, A. N. Balukhovsky, C. N. Wold, S. Flögel, E. Söding,
463 vaporites and the salinity of the ocean during the Phanerozoic: Implications for climate,
464 ocean circulation and life. *Palaeogeogr. Palaeoclimatol. Palaeoecol.*, **240**, 3-46 (2006).
46529. Y. Muramatsu, T. Doi, H. Tomaru, U. Fehn, Takeuchi, R., Matsumoto, R., Halogen
466 concentrations in pore waters and sediments of the Nankai Trough, Japan: Implications
467 for the origin of gas hydrates. *Appl. Geochem.*, **22**, 534-556 (2007).
46830. S. B. Jacobsen, G. J. Wasserburg, The mean age of mantle and crustal reservoirs. *J.*
469 *Geophys. Res.*, **84**, 7411–7427 (1979).
47031. A. W. Hofmann, Mantle geochemistry: the message from oceanic volcanism. *Nature*,
471 **385**, 219–229 (1997).
47232. R. K. Workman, S. R. Hart, Major and trace element composition of the depleted MORB
473 mantle (DMM). *Earth Planet. Sci. Lett.*, **231**, 53-72 (2005).
47433. M. A. Kendrick, M. Honda, T. Pettke, M. Scambelluri, D. Phillips, A. Giuliani,
475 Subduction zone fluxes of halogens and noble gases in seafloor and forearc serpentinites.
476 *Earth Planet. Sci. Lett.,* **365**, 86–96 (2013).
47734. R. O. Pepin, D. Porcelli, Xenon isotope systematics, giant impacts, and mantle degassing
478 on the early Earth. *Earth Planet. Sci. Lett.,* **250**, 470-485 (2006).

47935. P. J. Wallace, A. F. Anderson, “Volatiles in magmas” in Encyclopedia of Volcanoes,
480 H. Sigurdsson, Eds, Wiley, New York (2000), pp. 149-163.
48136. J. Korenaga, Hadean geodynamics and the nature of early continental crust. *Precambrian*
482 *Res.*, **359**, 106178 (2021).
48337. J. Korenaga, N. J. Planavsky, D. A. Evans, Global water cycle and the coevolution of the
484 Earth’s interior and surface environment. *Phil. Trans. R. Soc. A,* **375**, 20150393, 2017.
48538. R. Parai, S. Mukhopadhyay, Xenon isotopic constraints on the history of volatile
486 recycling into the mantle. *Nature*, **560**, 223-227 (2018).
48739. B. M. Urann, V. Le Roux, K. Hammond, H. R. Marshall, C.-T. A. Lee, B. D.
488 Monteleone, Fluorine and chlorine in mantle minerals and the halogen budget of the
489 Earth’s mantle. *Contrib. Mineral. Petrol.*, **172**, 51 (2017).
49040. E. Ito, D. M. Harris, A. T. Anderson Jr, Alteration of oceanic crust and geologic cycling
491 of chlorine and water. *Geochim. Cosmochim. Acta*, **47**, 1613-1624 (1983).
49241. N. H. Sleep, K. Zahnle, Carbon dioxide cycling and implications for climate on ancient
493 Earth. *J. Geophys. Res. Planets*, **106**, 1373-1399 (2001).
49442. M. M. Hirschmann, Comparative deep Earth volatile cycles: The case for C recycling
495 from exosphere/mantle fractionation of major (H_2O, C, N) volatiles and from H_2O/Ce,
496 CO_2/Ba, and CO_2/Nb exosphere ratios. *Earth Planet. Sci. Lett.,* **502**, 262-273 (2018).
49743. T. Kagoshima, Y. Sano, N. Takahata, T. Maruoka, T. P. Fischer, K. Hattori, Sulphur
498 geodynamic cycle. *Sci. Rep.*, **5**, 1-6 (2015).
49944. A. Mallik, Y. Li, M. Wiedenbeck, Nitrogen evolution within the Earth’s atmosphere-
500 mantle system assessed by recycling in subduction zones. *Earth Planet. Sci. Lett.,* **482**,
501 556-565 (2018).
50245. R. A. Feely, S. C. Doney, S. R. Cooley, Ocean acidification: Present conditions and
503 future changes in a high-CO_2 world. *Oceanography*, **22**, 36-47 (2009).
50446. W. Runguphan, X. Qu, S. E. O’connor, Integrating carbon-halogen bond formation into
505 medicinal plant metabolism. *Nature*, **468**, 461-464 (2010).
50647. J. L. Palandri, Y. K. Kharaka, A compilation of rate parameters of water-mineral
507 interaction kinetics for application to geochemical modeling. *US Geol. Surv. Open File*
508 *Report,* 2004-1068 (2004).

48. F. Robert, M. Chaussidon, A palaeotemperature curve for the Precambrian oceans based on silicon isotopes in cherts. *Nature*, **443**, 969–972 (2006).
49. J. P. Grotzinger, J. F. Kasting, New constraints on Precambrian ocean composition, *J. Geol.*, **101**, 235-243 (1993).
50. S. Kempe, E. T. Degens, An early soda ocean? *Chem. Geol.*, **53**, 95-108 (1985).
51. I. Halevy, A. Bachan, The geologic history of seawater pH. *Science*, **355**, 1069-1071 (2017).
52. J. Krissansen-Totton, G. N. Arney, D. C. Catling, Constraining the climate and ocean pH of the early Earth with a geological carbon cycle model. *Proc. Nati. Acad. Sci.U.S.A.*, **115**, 4105-4110 (2018).
53. C. H. Langumuir, E. M. Klein, T. Plank, "Petrological systematics of mid-ocean ridge basalts: Constraints on melt generation beneath ocean ridges" in *Mantle Flow and Melt Generation at Mid-Ocean Ridges*, J. P. Morgan, D. K. Blackman, J. M. Sinton, Eds, AGU Monograph (1992), pp. 183-280.
54. C. Dalou, K. T. Koga, N. Shimizu, J. Boulon, J. L. Devidal, Experimental determination of F and Cl partitioning between lherzolite and basaltic melt. *Contrib. Mineral. Petrol.*, **163**, 591-609 (2012).
55. C. Dalou, K. T. Koga, M. Le Voyer, N. Shimizu, Contrasting partition behavior of F and Cl during hydrous mantle melting: implications for Cl/F signature in arc magmas. *Prog. Earth Planet. Sci.*, **1**, 1-17 (2014).

Figures Legends

Figure 1. Covariations of F vs K during mantle melting and fractional crystallization. (A) Logarithmic concentrations of F vs. K in primary melt generated from the source mantle of MORB through partial melting. Different line colors correspond to different element bulk distribution coefficients during fractional crystallization. f_C is melt fraction during fractional crystallization. Black dot represents a sample composition of MORB. (B) Logarithmic concentrations of F vs. K in the source mantle of MORB. Different line colors correspond to different element bulk distribution coefficients during mantle melting. f_M is melt fraction. Black dots are sample primary melt compositions taken from (A). Grey bar and dotted rectangle are K concentration range (*25*) and the calculated F concentration range in the source mantle of MORB, respectively. Blue dashed line and blue dot represent the results of the log-log linear model. (C) Comparison between the constant ratio method and the method based on a log-log linear model, which are shown in green and blue, respectively. Orange dots are the MORB data of F and K concentrations from PetDB (*21*). Grey bar is the K concentration range in the source mantle of MORB (*25*).

Figure 2. Selected covariations between halogens and reference elements and their corresponding log-log linear models in MORB and OIB. (A) F vs. K, (B) Cl vs. Rb, (C) Br vs. Nb, and (D) I vs. Th in MORB. Orange dots are MORB data from PetDB (*21*). Bule solid and dashed lines are log-log linear models and their uncertainty ranges, respectively. Yellow bars and yellow dots represent the concentrations of reference elements and halogens, respectively, in the depleted MORB-source mantle (DMM). Figs. (E) to (H) are the same with (A) to (D), but for OIB data, shown as yellow dots, from PetDB (*21*). Green solid and dashed lines are log-log linear models and their uncertainty ranges, respectively. Blue bars and blue dots represent the concentrations of reference elements and halogens, respectively, in the enriched OIB-source mantle (EM).

552 **Figure 3.** CI-chondrite and Mg-normalized BSE abundance as a function of 50% condensation
553 temperature (T_c). Blue dots are element concentrations in BSE (*12*) normalized to CI-chondrite and Mg.
554 Yellow, green, blue, and pink bars represent the trend of moderately to highly volatile lithophile elements,
555 moderately siderophile elements, highly siderophile elements, and chalcophile elements, respectively.
556 Green dots are previous estimate of halogen concentration in BSE (*9*) normalized to CI-chondrite and Mg
557 (*11*). Red dots are our new estimates of halogen concentration in BSE normalized to CI-chondrite and Mg
558 (*11*). Yellow dots are our estimates of halogen concentration in BSE normalized to the CI-chondrite
559 composition of Clay et al. (*7*) and Mg. Values of 50% T_C are taken from Lodders (*14*).

560 **Table 1.** Halogen abundances in Earth's reservoirs, with the assumption that EM is the source
561 mantle of OIB.

	Mass (kg)	F (ppm)	Cl (ppm)	Br (ppb)	I (ppb)
Seawater (*9*)	1.40×10^{21}	1.3	1.93×10^{4}	6.6×10^{4}	60
Evaporites (*28*)	3.00×10^{19}	10	5.5×10^{5}	1.5×10^{5}	1.0×10^{3}
Crustal brines (*26, 27)*	6.00×10^{19}	20	1.0×10^{5}	6.0×10^{5}	1.5×10^{4}
Marine sediments (*29*)	5.00×10^{20}	1000	4.0×10^{3}	4.0×10^{4}	3.0×10^{4}
Continental crust (*24)*	2.09×10^{22}	553	244	880	700
Enriched OIB-source mantle (EM)	$1.21^{+0.8}_{-0.8} \times 10^{24}$	68^{+20}_{-16}	175^{+79}_{-55}	93^{+44}_{-30}	$2.2^{+0.81}_{-0.59}$
Depleted MORB-source mantle (DMM)	$2.81^{+0.8}_{-0.8} \times 10^{24}$	$48^{+5.3}_{-4.8}$	$26^{+10}_{-6.9}$	32^{+8}_{-6}	$0.5^{+0.10}_{-0.09}$
Depleted mantle (DM)	4.02×10^{24}	$54^{+4.8}_{-4.4}$	67^{+26}_{-19}	49^{+10}_{-8}	$1.0^{+0.14}_{-0.12}$
BSE (This study)	4.04×10^{24}	$57^{+4.8}_{-4.4}$	81^{+24}_{-19}	91^{+19}_{-14}	$8.6^{+0.70}_{-0.61}$
Degassed from DM (This study)	-	5.24%	17.30%	46.59%	88.20%
BSE (*9*)	4.04×10^{24}	17 ± 6	26 ± 8	76 ± 25	7 ± 4
Degassed from DM (*9*)	-	51.08%	86.67%	88.14%	97.03%

562

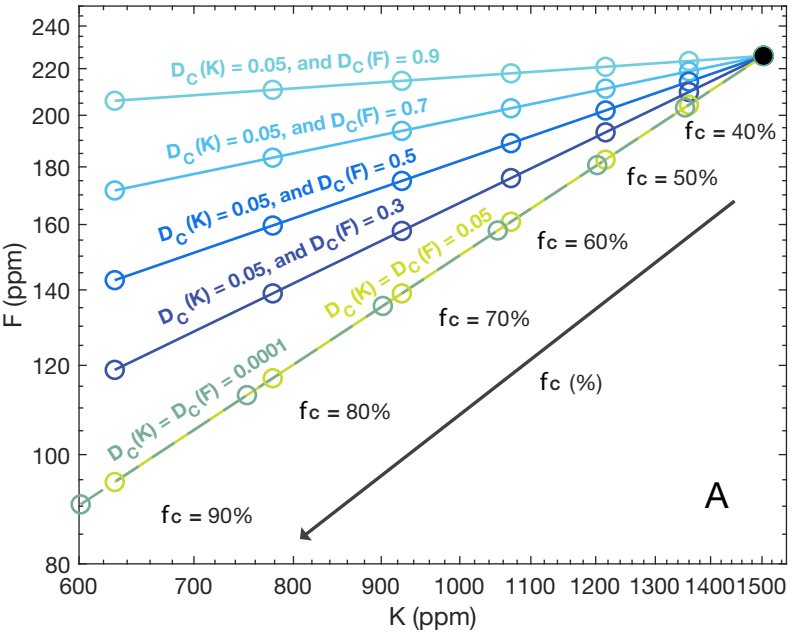
$D_C(K) = 0.05$, and $D_C(F) = 0.9$
$D_C(K) = 0.05$, and $D_C(F) = 0.7$
$D_C(K) = 0.05$, and $D_C(F) = 0.5$
$D_C(K) = 0.05$, and $D_C(F) = 0.3$
$D_C(K) = D_C(F) = 0.05$
$D_C(K) = D_C(F) = 0.0001$
fc = 40%
fc = 50%
fc = 60%
fc = 70%
fc = 80%
fc = 90%
fc (%)
A
F (ppm)
K (ppm)

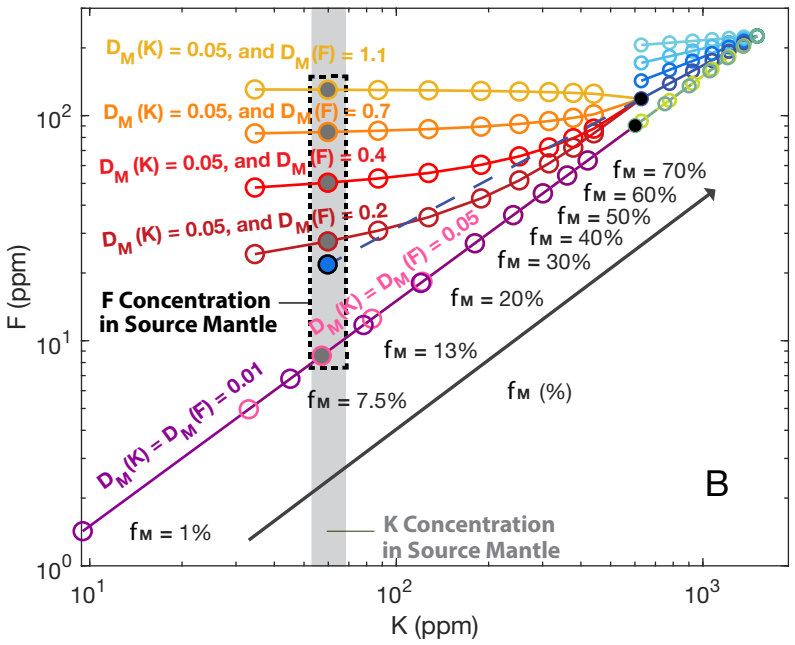
$D_M(K) = 0.05$, and $D_M(F) = 1.1$
$D_M(K) = 0.05$, and $D_M(F) = 0.7$
$D_M(K) = 0.05$, and $D_M(F) = 0.4$
$D_M(K) = 0.05$, and $D_M(F) = 0.2$
$D_M(K) = D_M(F) = 0.05$
$D_M(K) = D_M(F) = 0.01$
F Concentration in Source Mantle
K Concentration in Source Mantle
fM = 70%
fM = 60%
fM = 50%
fM = 40%
fM = 30%
fM = 20%
fM = 13%
fM = 7.5%
fM = 1%
fM (%)
B
F (ppm)
K (ppm)

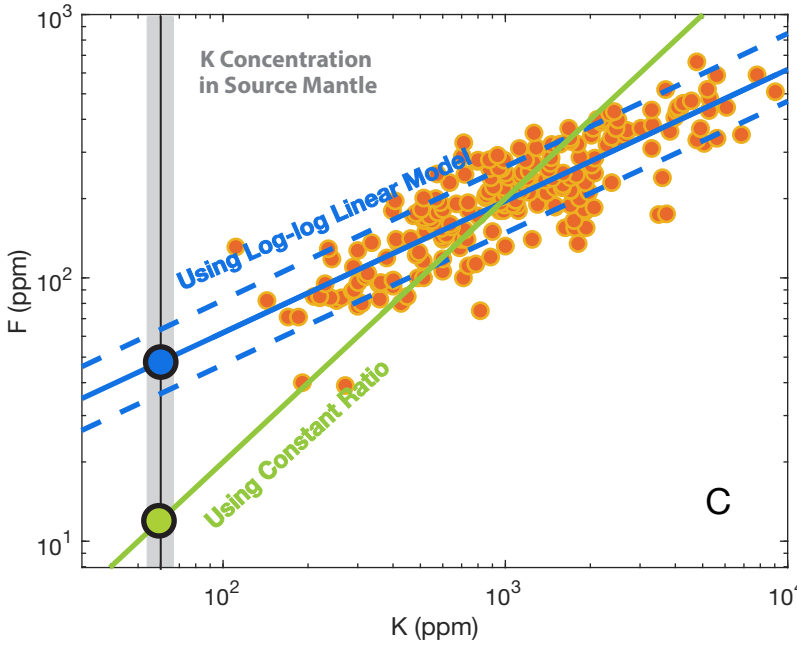
K Concentration in Source Mantle
Using Log-log Linear Model
Using Constant Ratio
C
F (ppm)
K (ppm)

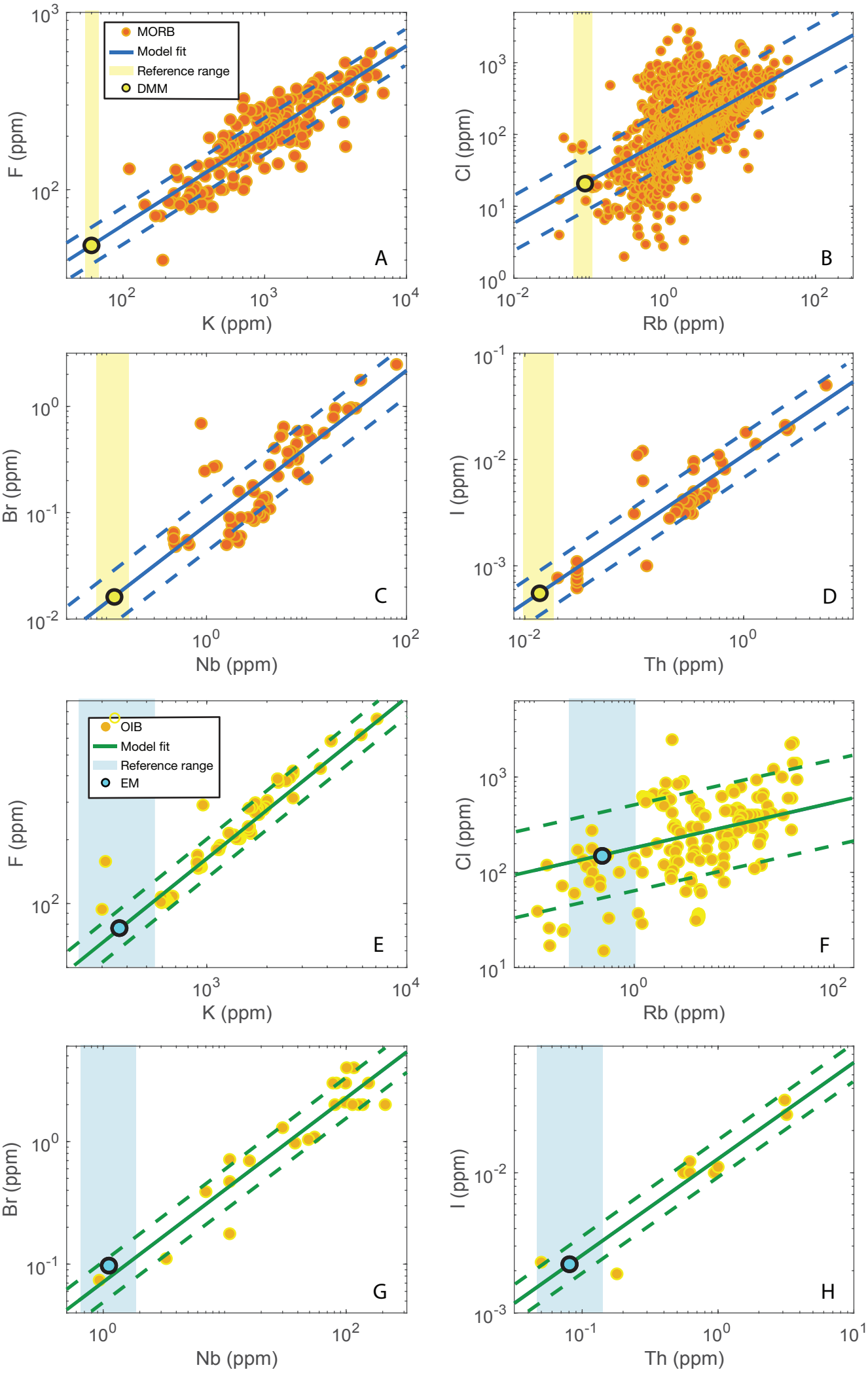
MORB
Model fit
Reference range
DMM
F (ppm)
K (ppm)
A
Cl (ppm)
Rb (ppm)
B
Br (ppm)
Nb (ppm)
C
I (ppm)
Th (ppm)
D
OIB
Model fit
Reference range
EM
F (ppm)
K (ppm)
E
Cl (ppm)
Rb (ppm)
F
Br (ppm)
Nb (ppm)
G
I (ppm)
Th (ppm)
H

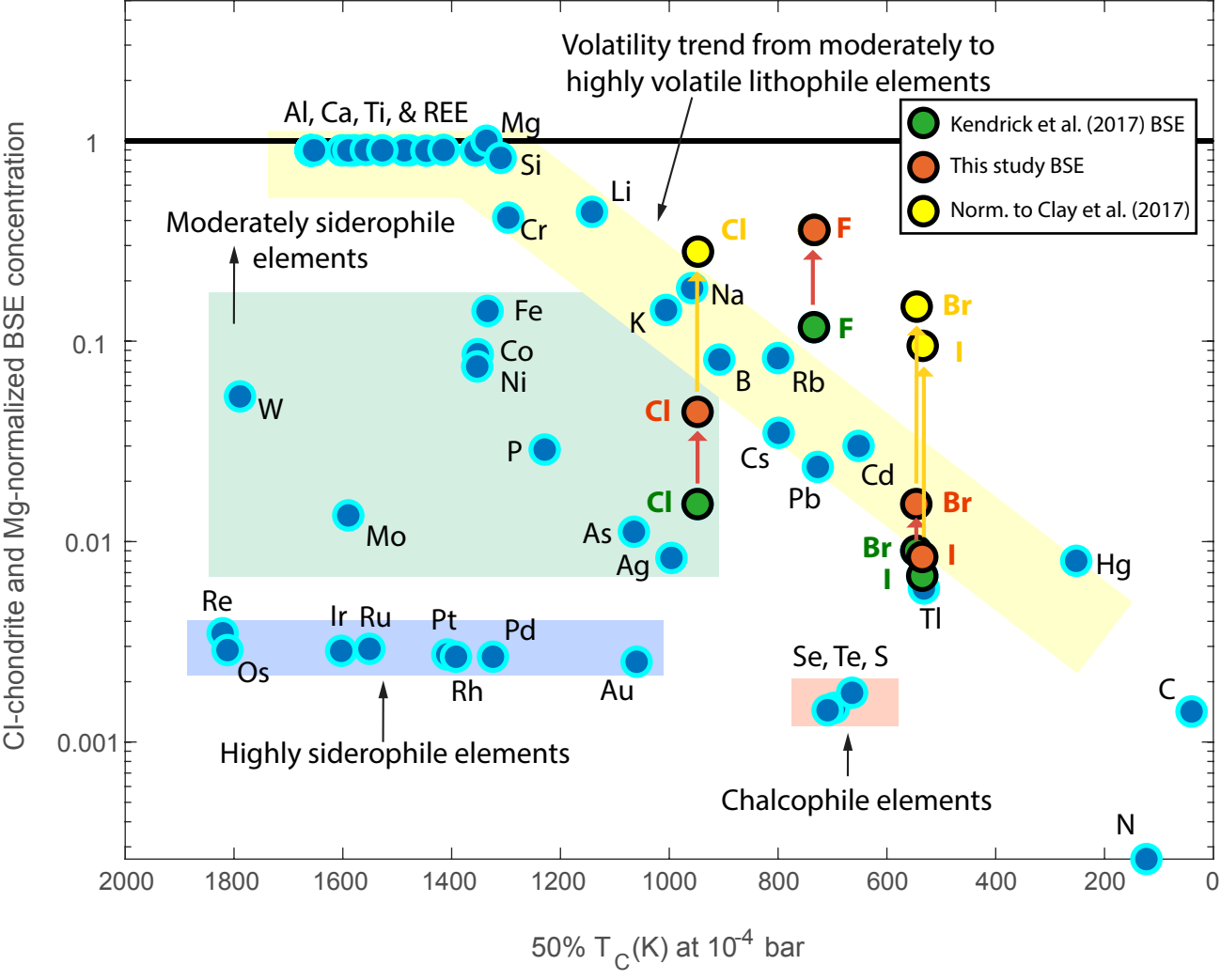
Volatility trend from moderately to highly volatile lithophile elements
Kendrick et al. (2017) BSE
This study BSE
Norm. to Clay et al. (2017)
Al, Ca, Ti, & REE
Mg
Si
Li
Cr
Moderately siderophile elements
Fe
Co
Ni
W
P
Mo
Cl
Na
K
B
Rb
Cs
Pb
Cd
As
Ag
F
Br
I
Hg
Tl
Re
Os
Ir
Ru
Pt
Rh
Pd
Au
Highly siderophile elements
Se, Te, S
Chalcophile elements
C
N
CI-chondrite and Mg-normalized BSE concentration
50% T$_C$(K) at 10^{-4} bar
1
0.1
0.01
0.001
2000
1800
1600
1400
1200
1000
800
600
400
200
0

Table 1. Halogen abundances in Earth's reservoirs, with the assumption that EM is the source mantle of OIB.

	Mass (kg)	F (ppm)	Cl (ppm)	Br (ppb)	I (ppb)
Seawater (*9*)	1.40×10^{21}	1.3	1.93×10^{4}	6.6×10^{4}	60
Evaporites (*28*)	3.00×10^{19}	10	5.5×10^{5}	1.5×10^{5}	1.0×10^{3}
Crustal brines (*26, 27*)	6.00×10^{19}	20	1.0×10^{5}	6.0×10^{5}	1.5×10^{4}
Marine sediments (*29*)	5.00×10^{20}	1000	4.0×10^{3}	4.0×10^{4}	3.0×10^{4}
Continental crust (*24*)	2.09×10^{22}	553	244	880	700
Enriched OIB-source mantle (EM)	$1.21^{+0.8}_{-0.8} \times 10^{24}$	68^{+20}_{-16}	175^{+79}_{-55}	93^{+44}_{-30}	$2.2^{+0.81}_{-0.59}$
Depleted MORB-source mantle (DMM)	$2.81^{+0.8}_{-0.8} \times 10^{24}$	$48^{+5.3}_{-4.8}$	$26^{+10}_{-6.9}$	32^{+8}_{-6}	$0.5^{+0.10}_{-0.09}$
Depleted mantle (DM)	4.02×10^{24}	$54^{+4.8}_{-4.4}$	67^{+26}_{-19}	49^{+10}_{-8}	$1.0^{+0.14}_{-0.12}$
BSE (This study)	4.04×10^{24}	$57^{+4.8}_{-4.4}$	81^{+24}_{-19}	91^{+19}_{-14}	$8.6^{+0.70}_{-0.61}$
Degassed from DM (This study)	-	5.24%	17.30%	46.59%	88.20%
BSE (*9*)	4.04×10^{24}	17 ± 6	26 ± 8	76 ± 25	7 ± 4
Degassed from DM (*9*)	-	51.08%	86.67%	88.14%	97.03%

PNAS
www.pnas.org

Supplementary Information for

A New Halogen Budget of Bulk Silicate Earth Points to a History of Early Halogen Degassing Followed by Net Regassing

Meng Guo[1], Jun Korenaga[1]

[1]Department of Earth and Planetary Sciences, Yale University, New Haven, CT, USA.

Corresponding author: Meng Guo
Email: meng.guo@yale.edu

This PDF file includes:

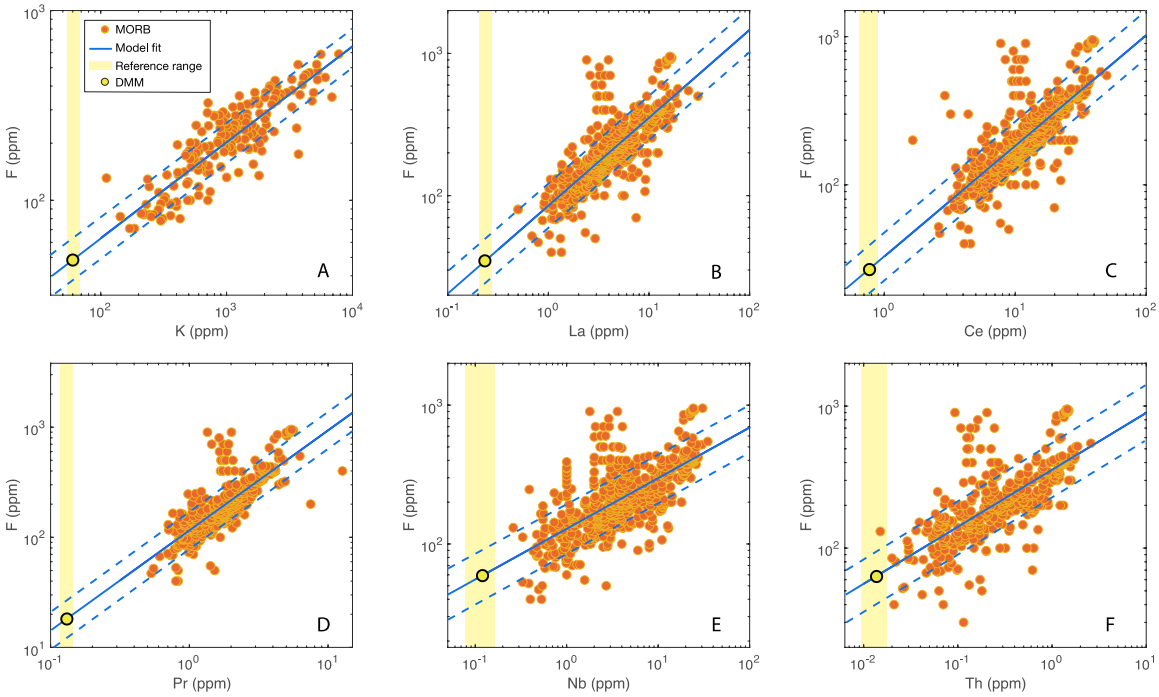

Fig. S1. Selected covariations between fluorine and reference elements in MORB, and their corresponding log-log linear models. (A) F vs. K, (B) F vs. La, (C) F vs. Ce, (D) F vs. Pr, (E) F vs. Nb, and (F) F vs. Th. Concentrations are in the unit of ppm. Orange dots are the MORB data from PetDB *(1)*. Bule solid and dashed lines are log-log linear models and their uncertainties, respectively. Yellow bars and yellow dots represent the concentrations of reference elements and fluorine, respectively, in the depleted MORB-source mantle (DMM).

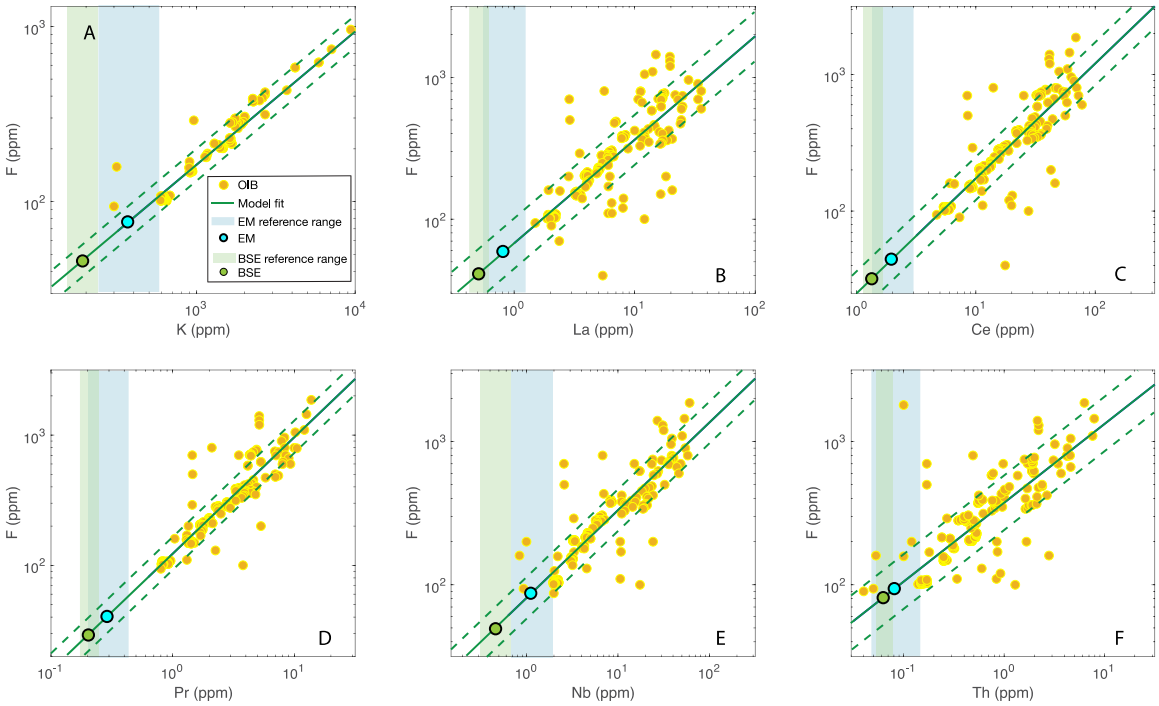

Fig.S2. Same as Fig. 2, but for OIB data, shown as yellow dots, from PetDB *(1)*. Green solid and dashed lines are log-log linear models and their uncertainties, respectively. Blue bars and dots represent the concentration of reference elements and fluorine, respectively, in the enriched OIB-source mantle (EM). Green bars and dots represent the concentrations of reference elements and fluorine, respectively, in the bulk silicate Earth (BSE); this corresponds to the assumption that OIB is directly derived from BSE (primitive mantle).

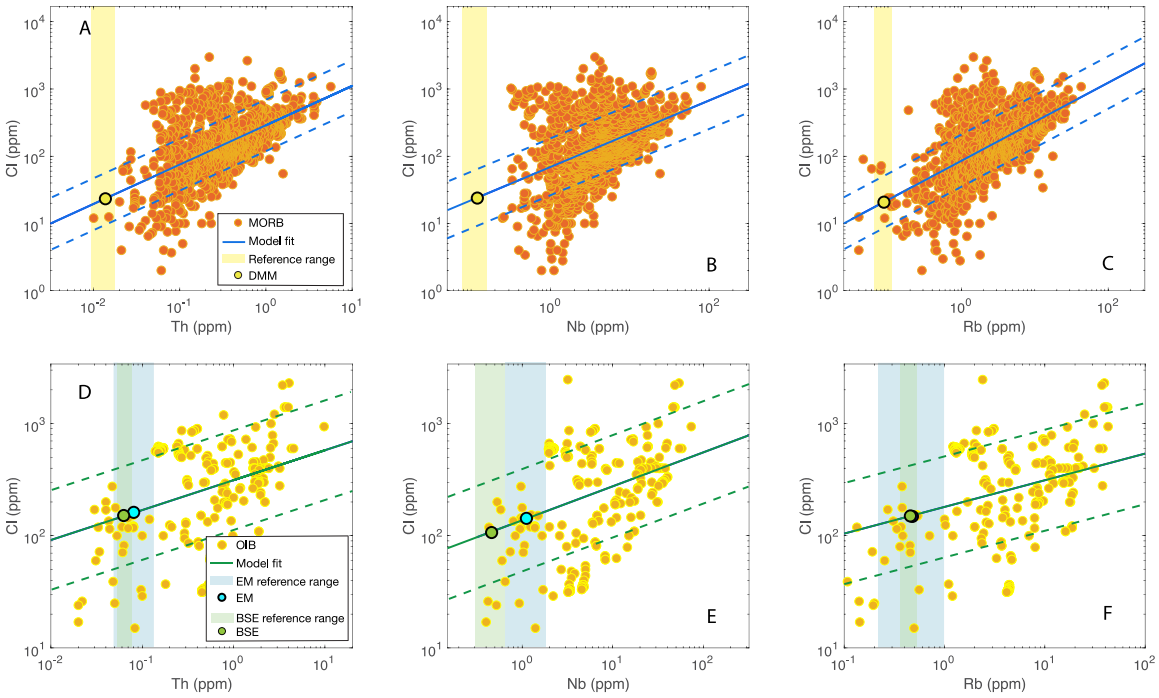

Fig. S3. Same as Figs. 1 and 2, but for chlorine in MORB and OIB, from PetDB *(1)*. (A) Cl vs. Th, (B) Cl vs. Nb, and (C) Cl vs. Rb in MORB; (D) Cl vs. Th, (E) Cl vs. Nb, and (F) Cl vs. Rb in OIB.

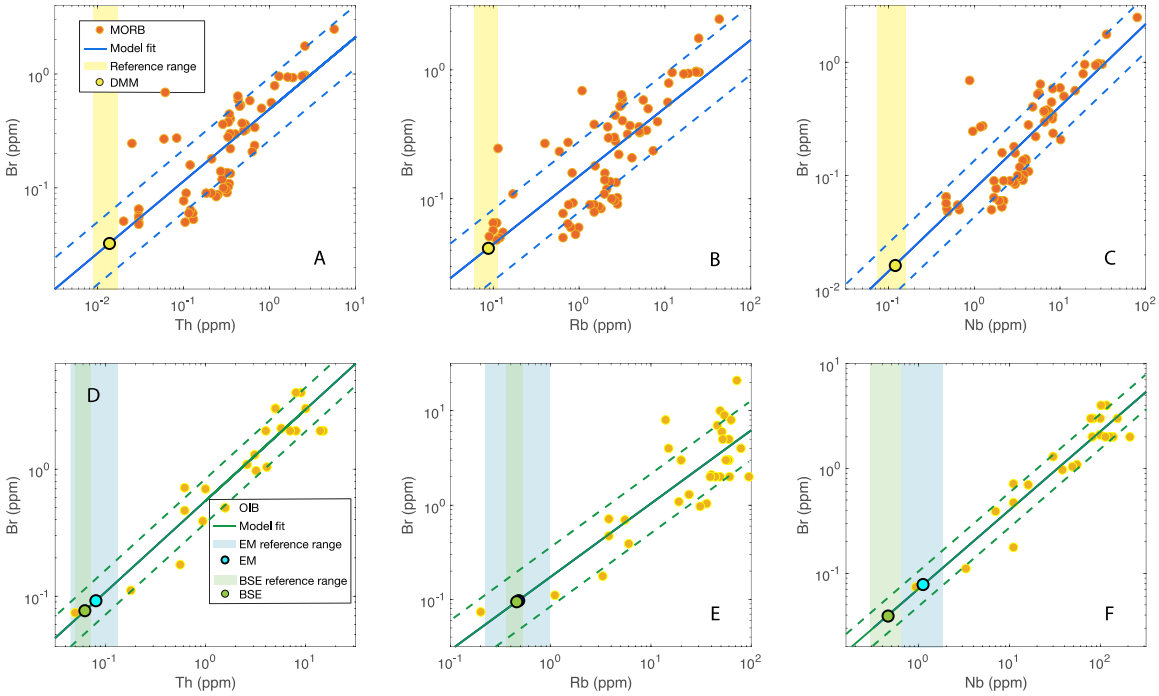

Fig. S4. Same as Figs. 1 and 2, but for bromine in MORB and OIB, from PetDB *(1).* (A) Br vs. Th, (B) Br vs. Rb, and (C) Br vs. Nb in MORB; (D) Br vs. Th, (E) Br vs. Rb, and (F) Br vs. Nb in OIB.

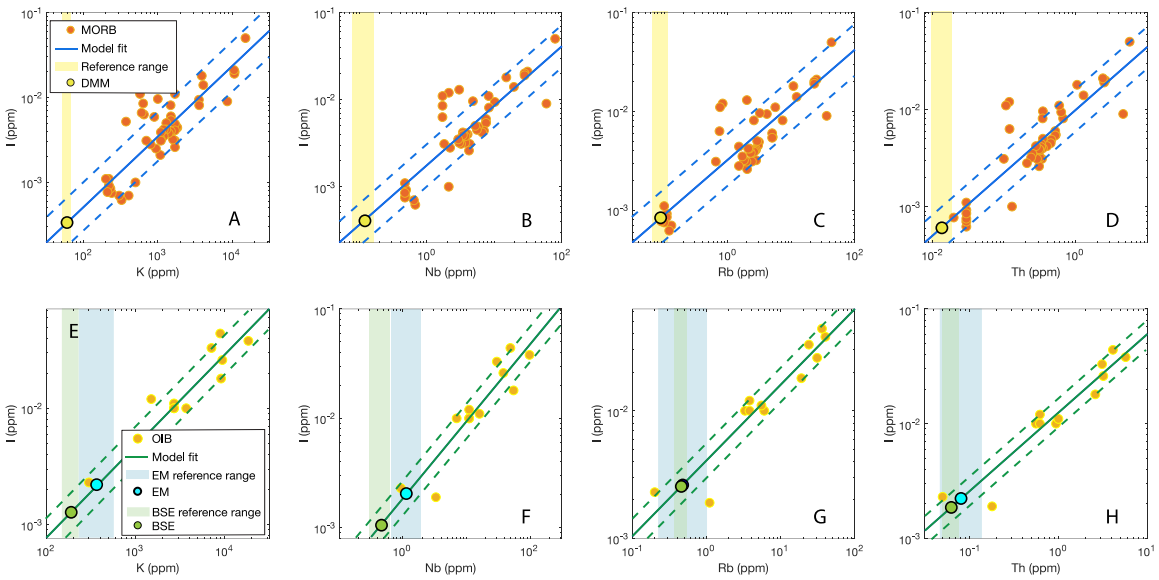

Fig. S5. Same as Figs. 1 and 2, but for iodine in MORB and OIB, from PetDB *(1)*. (A) I vs. K, (B) I vs. Nb, (C) I vs. Rb, and (D) I vs. Th in MORB; (E) I vs. K, (F) I vs. Nb, (G) I vs. Rb, and (H) I vs. Th in OIB.

Table S1. Logarithmic slopes and correlation coefficients of halogens and reference elements in MORB. Data from PetDB *(1). N* is the number of relevant data. Reference elements are selected according to the following two criteria: (1) they have sufficiently high correlation in the log-log space with halogen in both MORB and OIB, and (2) they have well-constrained abundances in DMM, CC, and BSE. The selected element pairs used in this study are marked in bold. In general, most elements (REE, Sr, Zr, and P) are not selected due to their low logarithm correlation coefficients with halogens in either MORB or OIB or both, whereas others (e.g., Br) are due to their lack of constraints in DMM, CC, or BSE.

MORB	*N*	Log. Corr. coefficient	Log. slope	Reason for not selected*
F / K	**187**	**0.87**	**0.67**	**-**
F / La	**521**	**0.80**	**0.62**	**-**
F / Ce	**514**	**0.78**	**0.75**	**-**
F / Pr	**428**	**0.80**	**0.91**	**-**
F / Nd	521	0.74	1.07	3
F / Sm	535	0.60	1.14	2
F / Eu	522	0.64	1.31	2
F / Gd	580	0.50	0.55	2
F / Tb	492	0.02	0.03	1
F / Dy	452	0.35	0.93	1
F / Ho	438	0.27	0.92	1
F / Er	452	0.23	0.61	1
F / Tm	384	0.14	0.31	1
F / Yb	521	0.14	0.31	1
F / Lu	506	0.15	0.35	1
F / Nb	**570**	**0.74**	**0.37**	**-**
F / Rb	554	0.60	0.31	2
F / Th	**429**	**0.75**	**0.40**	**-**
Cl / K	732	0.58	0.85	3
Cl / La	1367	0.45	0.71	1
Cl / Ce	1361	0.42	0.78	1
Cl / Pr	1139	0.39	0.83	1
Cl / Nd	1256	0.37	0.91	1
Cl / Sm	1423	0.29	0.93	1
Cl / Eu	1254	0.25	0.91	1
Cl / Gd	1335	0.12	0.30	1
Cl / Tb	1174	0.30	0.92	1
Cl / Dy	1166	0.28	1.35	1
Cl / Ho	1086	0.25	1.19	1
Cl / Er	1190	0.11	0.46	1
Cl / Tm	935	0.10	0.26	1
Cl / Yb	1260	0.10	0.43	1
Cl / Lu	1194	0.21	0.92	1
Cl / Nb	**1184**	**0.54**	**0.50**	**-**
Cl / Rb	**1476**	**0.61**	**0.63**	**-**
Cl / Th	**1325**	**0.54**	**0.58**	**-**
Cl / Br	226	0.97	1.04	4

Table S1. (continued)

MORB	*N*	Log. Corr. coefficient	Log. slope	Reason for not selected*
Br / K	50	0.31	0.99	2
Br / La	83	0.74	0.82	3
Br / Ce	69	0.75	1.01	3
Br / Pr	57	0.59	1.18	1
Br / Nd	70	0.61	1.11	1
Br / Sm	95	0.44	1.37	1
Br / Eu	82	0.48	1.39	1
Br / Gd	76	0.38	1.42	1
Br / Tb	69	0.20	0.73	1
Br / Dy	28	-0.32	-1.53	1
Br / Ho	33	-0.16	-0.66	1
Br / Er	66	0.29	0.13	1
Br / Tm	14	-0.12	-0.36	1
Br / Yb	82	0.04	0.17	1
Br / Lu	79	0.05	0.20	1
Br / Nb	**65**	**0.83**	**0.73**	**-**
Br / Rb	**71**	**0.78**	**0.53**	**-**
Br / Th	**66**	**0.79**	**0.63**	**-**
I / K	**45**	**0.85**	**0.82**	**-**
I / La	45	0.77	0.91	2
I / Ce	45	0.74	1.04	2
I / Pr	34	0.66	1.53	2
I / Nd	45	0.69	1.32	2
I / Sm	58	0.51	1.41	2
I / Eu	44	0.62	1.87	2
I / Gd	56	0.21	0.43	2
I / Tb	44	0.34	1.34	2
I / Dy	41	0.47	2.12	2
I / Ho	10	0.49	2.17	1
I / Er	43	0.31	1.38	1
I / Tm	8	0.43	1.80	1
I / Yb	44	0.21	0.97	1
I / Lu	41	0.22	0.95	1
I / Nb	**43**	**0.86**	**0.73**	**-**
I / Rb	**44**	**0.84**	**0.58**	**-**
I / Th	**42**	**0.88**	**0.69**	**-**

* Reasons for not selected as reference element: 1: Low log. correlation in both MORB and OIB; 2: Low log. correlation in MORB; 3: Low log. correlation in OIB; 4: Not well-constrained in BSE, DMM, or CC.

Table S2. Logarithmic slopes and correlation coefficients of halogens and reference elements in OIB. Data from PetDB *(1). N* is the number of relevant data. Reference elements are selected according to the following two criteria: (1) they have sufficiently high correlation in the log-log space with halogen in both MORB and OIB, and (2) they have well-constrained abundances in DMM, CC, and BSE. The selected element pairs used in this study are marked in bold. In general, most elements (REE, Sr, Zr, and P) are not selected due to their low logarithm correlation coefficients with halogens in either MORB or OIB or both, whereas others (e.g., Br) are due to their lack of constraints in DMM, CC, or BSE.

OIB	*N*	Log. Corr. coefficient	Log. slope	Reason for not selected*
F / K	**121**	**0.92**	**0.76**	**-**
F / La	**188**	**0.83**	**0.73**	**-**
F / Ce	**187**	**0.87**	**0.84**	**-**
F / Pr	**179**	**0.92**	**0.89**	**-**
F / Nd	195	0.50	0.59	3
F / Sm	197	0.76	1.12	2
F / Eu	180	0.76	1.21	2
F / Gd	181	0.81	1.36	2
F / Tb	178	0.70	1.25	1
F / Dy	181	0.53	1.13	1
F / Ho	164	0.62	1.38	1
F / Er	180	0.46	1.15	1
F / Tm	163	0.53	1.31	1
F / Yb	180	0.26	0.65	1
F / Lu	181	0.23	0.58	1
F / Nb	**183**	**0.89**	**0.61**	**-**
F / Rb	185	0.83	0.57	2
F / Th	**184**	**0.81**	**0.55**	**-**
Cl / K	139	-0.28	-0.50	3
Cl / La	255	0.29	0.48	1
Cl / Ce	252	0.34	0.64	1
Cl / Pr	214	0.33	0.65	1
Cl / Nd	244	0.13	0.22	1
Cl / Sm	255	0.44	1.66	1
Cl / Eu	243	-0.01	-0.02	1
Cl / Gd	224	-0.08	-0.20	1
Cl / Tb	221	-0.13	-0.39	1
Cl / Dy	242	-0.36	-1.72	1
Cl / Ho	195	-0.39	-1.32	1
Cl / Er	242	-0.37	-2.13	1
Cl / Tm	185	-0.51	-1.98	1
Cl / Yb	241	-0.40	-1.69	1
Cl / Lu	231	-0.41	-1.65	1
Cl / Nb	**232**	**0.51**	**0.31**	**-**
Cl / Rb	**234**	**0.58**	**0.58**	**-**
Cl / Th	**232**	**0.56**	**0.30**	**-**
Cl / Br	12	0.99	0.94	4

Table S2. (continued)

OIB	*N*	Log. Corr. coefficient	Log. slope	Reason for not selected*
Br / K	9	0.83	0.79	2
Br / La	13	0.46	1.02	3
Br / Ce	13	0.36	0.91	3
Br / Pr	13	0.38	0.99	1
Br / Nd	13	0.36	1.14	1
Br / Sm	13	0.23	0.93	1
Br / Eu	13	0.13	0.64	1
Br / Gd	13	-0.03	0.13	1
Br / Tb	13	-0.31	-1.65	1
Br / Dy	13	-0.50	-2.61	1
Br / Ho	4	-0.65	-5.75	1
Br / Er	13	-0.75	-3.62	1
Br / Tm	4	-0.39	-1.86	1
Br / Yb	13	-0.80	-4.53	1
Br / Lu	13	-0.75	-4.59	1
Br / Nb	**23**	**0.94**	**0.75**	**-**
Br / Rb	**30**	**0.83**	**0.78**	**-**
Br / Th	**23**	**0.93**	**0.72**	**-**
I / K	**9**	**0.90**	**0.82**	**-**
I / La	9	0.93	0.98	2
I / Ce	9	0.93	1.11	2
I / Pr	9	0.93	1.23	2
I / Nd	9	0.92	1.38	2
I / Sm	9	0.92	1.77	2
I / Eu	9	0.93	2.27	2
I / Gd	9	0.92	2.37	2
I / Tb	9	0.88	3.01	2
I / Dy	9	0.84	3.51	2
I / Ho	0	-	-	1
I / Er	9	0.56	3.46	1
I / Tm	0	-	-	1
I / Yb	9	0.12	0.77	1
I / Lu	9	-0.22	-1.01	1
I / Nb	**9**	**0.92**	**0.78**	**-**
I / Rb	**9**	**0.93**	**0.58**	**-**
I / Th	**9**	**0.94**	**0.69**	**-**

* Reasons for not selected as reference element: 1: Low log. correlation in both MORB and OIB; 2: Low log. correlation in MORB; 3: Low log. correlation in OIB; 4: Not well-constrained in BSE, DMM, or CC.

Table S3. Halogen abundances in Earth's silicate reservoirs, with the assumption that BSE is the source mantle of OIB.

	Mass (kg)	F (ppm)	Cl (ppm)	Br (ppb)	I (ppb)
BSE (assume BSE is the source mantle of OIB)	4.04×10^{24}	$51^{+5.1}_{-4.6}$	157^{+67}_{-47}	73^{+18}_{-14}	$1.7^{+0.20}_{-0.18}$
Degassed from DM	-	5.85%	8.93%	58.08%	446.19%

SI References

1. The data were downloaded from the PetDB Database (https://search.earthchem.org/) on 25th Jan, 2021.